

# Testing model independent modified gravity with future large scale surveys

Daniel B. Thomas\* and Carlo R. Contaldi

*Theoretical Physics, Blackett Laboratory, Imperial College, London*

(Dated: November 17, 2022)

Model-independent parametrisations of modified gravity have attracted a lot of attention over the past few years and numerous combinations of experiments and observables have been suggested to constrain the parameters used in these models. Galaxy clusters have been mentioned, but not looked at as extensively in the literature as some other probes. Here we look at adding galaxy clusters into the mix of observables and examine how they could improve the constraints on the modified gravity parameters. In particular, we forecast the constraints from combining Planck satellite Cosmic Microwave Background (CMB) measurements and Sunyaev–Zeldovich (SZ) cluster catalogue with a DES-like Weak Lensing (WL) survey. We find that cluster counts significantly improve the constraints over those derived using CMB and WL. We then look at surveys further into the future, to see how much better it may be feasible to make the constraints.

PACS numbers: 04.80.Cc,98.65.Cw,98.80.-k

## I. INTRODUCTION

Einstein’s General Relativity (GR) is one of the principal ingredients of modern cosmology. Indeed, it could be argued that it was only with the development of GR that cosmology really became a part of physics. Nonetheless, it is our job as physicists to continue to test even the most fundamental pillars of cosmology in order to refine, improve and further justify our model of the universe. There are also fundamental reasons for considering different theories of gravity: GR is inconsistent with quantum mechanics and the search for a theory of ‘Quantum Gravity’ is one of the holy grails of modern physics.

It has proved to be difficult to test GR outside of the solar system, particularly as the effects of a different theory of gravity could be degenerate with behaviour induced by different constituents of the universe. This is the case with current observations that suggest the presence of some form of dark matter and dark energy. Dark matter is required to explain galaxy rotation curves, galaxy lensing, nucleosynthesis, acoustic oscillations in the CMB, and the growth of structure in the Universe to name a few. The requirement for dark energy is underpinned by observations of the background expansion rate and large scale structure measurement.

The question has often been raised as to whether these effects could be due to a modified gravity theory. Proposals for such a theory include a number of  $f(R)$  theories, the Dvali Gabadadze Porrati (DGP) model [1], conformal gravity [2], Modified Newtonian dynamics (MOND) [3] and its covariant, relativistic extensions [4], and Einstein Aether theories [5], (see also the recent review [6] for an exhaustive list of candidates). It is possible, if GR is indeed the correct theory of gravity, that this debate will only be settled by the non-gravitational detection of the dark matter and/or dark energy. However, since we

do not know whether or not GR is indeed the correct theory of gravity, it seems reasonable to consider which observations could allow us to detect modified gravity.

More importantly, are there ways to test deviations from GR in a model independent way? There are several advantages to a model independent approach; some alternatives to GR do exist but there is no complete theory of, for example, quantum gravity to draw on. Also, there are no ‘stand-out’ candidates that are universally considered to be strong alternatives. Another advantage of a model independent approach is that the results do not rely on model selection techniques such as  $\chi^2$  per degree of freedom or other ways of choosing between competing theories. Thus, they also do not rely on us having *the* correct theory to hand. A result that is inconsistent with the GR based, concordance cosmology will be unambiguous and therefore a strong motivator to develop alternative theories, as well as possibly giving us a clue as to the nature of these theories.

There have been many recent studies looking at model independent tests of the dark energy/cold dark matter ( $\Lambda$ CDM) paradigm in GR. These can be roughly split into two categories: consistency checks of the  $\Lambda$ CDM assumption [7–9] and those that introduce new parameters to evaluate the level of deviation from GR (see [6] for a complete review of the literature). These parametrisations and consistency checks have considered the majority of cosmological observations: weak lensing, the CMB, particularly through its Integrated Sachs Wolfe (ISW) effect, Baryon Acoustic Oscillations (BAO), SN1a Supernovae luminosity distance observations, cluster counts, and galaxy redshift and peculiar velocity surveys. The purpose is normally to constrain both the background expansion history and the perturbations, or growth of structure, around the background, with some observables being sensitive to both. The constraints are then combined. This approach works well because the growth and expansion are determined by the same quantities under the concordance cosmology and this is the basis for the consistency checks. A parameter that can be used

---

\*Electronic address: daniel.b.thomas08@imperial.ac.uk

without modifying gravity is  $\gamma$ , a parametrisation of the growth index [10, 11]:

$$\frac{d \ln D(k, a)}{d \ln a} = \Omega_m(a)^\gamma. \quad (1)$$

Here,  $D(k, z) = \delta(k, z)/\delta(k, z = \infty)$  where  $\delta$  is the matter density contrast. For  $\Lambda$ CDM,  $\gamma = 0.55$  is a good fit to the growth. With the modified gravity parametrisations, the parameters often relate to the two gravitational potentials  $\Psi$  and  $\Phi$  appearing in the perturbation to the Friedmann Roberston Walker (FRW) metric. Since different observations depend on different combinations of these potentials, combining several experiments gives the best constraints.

Constraints from current data have been examined (see [6] for a review) and the general conclusion appears to be that the concordance cosmology is consistent with all of the current data. However, the data available today does not have enough constraining power to rule out even relatively significant modifications to gravity and they are certainly not precise enough to distinguish *between* modified gravity theories. Work has also gone into forecasting future constraints on a number of theories and/or parametrisations of the modifications to GR [9, 12–19]. The consensus is that future surveys will greatly improve prospects with the expectation that a number of theories competing with GR will be ruled out.

Now is a good time to consider these issues as we are in an era where the observational front is rapidly advancing in the field. Most, if not all, of the current and future measurements can be brought to bear on the issue of modified gravity. We have had pioneering ground and space-based CMB experiments over the last 20 years and now await the data from the Planck satellite [20]. Weak lensing surveys of cosmic shear have also matured into a precise observational tool [21] and future, planned surveys promise to bring these measurements to the fore front of the data landscape with large scale surveys underway or in the development stage (e.g. PANSTARRS [22], DES [23], and LSST [24]). In addition large scale surveys of galaxy redshifts have already been carried out (SDSS [25], and 2DFGRS [26]) with even larger and deeper ones targeting BAO measurements to come.

So far, we have only mentioned modified gravity as an alternative to dark energy. The other alternative under consideration is whether the assumptions of homogeneity and isotropy are justified and hence whether using the FRW metric itself is justified. It is also important to note that measurements of the background expansion alone cannot distinguish between dark energy or modified gravity [27] and it has also been argued that measurements of perturbations may also suffer from this degeneracy if sufficiently complex models of perturbed dark energy are allowed [28].

In this work, we will only consider modified gravity and will look at how well some future experiments, particularly DES and CMB measurements and SZ cluster counts from Planck and its successors, will combine to constrain

certain modified gravity parameters that characterise potential deviations from GR.

In this *paper* we investigate how the combination of future observations of CMB, weak lensing (WL), and cluster counts (CC) are able to constrain the model independent parametrisation of modified gravity theories. We restrict ourselves to the simplest form of modified gravity with at most a linear redshift dependence in the modification and no scale dependence. These assumptions are fairly restrictive in terms of the physical mechanism that could underpin the modified phenomenology but provide a simple starting point for investigation into future constraints from different observables. In Section II we briefly review the model independent parametrisation of modified gravity used in this work. In Section III we describe the three observables used in our forecasts. In Section IV we review the Fisher matrix formalism used in our calculations and the experimental ‘Stages’ considered in our forecasts. Our results are presented in Section V and we conclude with a discussion of the results in Section VI.

## II. PARAMETRISED MODIFIED GRAVITY

There has been considerable discussion regarding the best ways to address and parametrise deviations from GR. Of course, it is always possible to calculate observables in the universe given a particular modified gravity model, and this has been done for several models:  $f(R)$ , DGP, Einstein Aether, TeVeS and conformal gravity have all been tested against cosmological data. However, it is useful to consider general kinds of deviations from GR that can then be used as a ‘null-test’ of the current paradigm. In other words, if there is significant evidence that the parameters we consider differ from their values under GR, then there is clearly a case that the current model is wrong that is not predicated on a particular modified gravity model.

Numerous sets of ‘modified gravity parameters’ (MGPs) have been suggested in the literature, see e.g. [29] for a partial translation table and [12] for a discussion of the differences with some of the parametrisations. Most of the parametrisations are phenomenological modifications to the Einstein equations and typically involve a parameter relating to the strength of gravity and a parameter relating the two scalar potentials in the metric.

In this work we will use two parameters,  $\eta$  and  $\mu$ , following [30]. The first,  $\eta$ , is the ratio of the two potentials,  $\eta = \Psi/\Phi$ . This will be roughly equal to unity in GR unless any of the particle species has large anisotropic stress, this is not expected to be the case unless a significant amount of dark matter is made up of massive neutrinos in conflict with Large Scale Structure (LSS) data. The second,  $\mu$ , is a modification of the poisson equation, and is essentially a time and space dependent Newton’s constant. Fourier expanding the spatial dependence with wavenumbers  $k$  and assuming isotropy, the modification

of the Poisson equation is as follows

$$k^2\Psi(a, k) = -4\pi G a^2 \mu(a, k) \rho(a) \Delta(a, k), \quad (2)$$

where,  $a$  is the FRW scale factor,  $G$  is Newton's constant,  $\rho$  is the background density of cold dark matter and  $\Delta$  is the gauge invariant density contrast given by

$$\Delta = \delta + \frac{3aHv}{k}, \quad (3)$$

where the cold dark matter density contrast is defined as  $\delta = \delta\rho(a, k)/\rho(a)$ ,  $v$  is velocity of the dark matter and  $H$  is the Hubble parameter.

The GR limit is recovered when the function  $\mu$  is constant and equal to unity. Note that we are using the potential  $\Psi$  in the Poisson equation since this determines the acceleration of non-relativistic particles. These MGPs have been included as parameters in the modified Einstein-Boltzmann code `MGCAMB` [30] based on the well-known `CAMB` [31] package for integrating photon and matter perturbations. This parametrisation can be related directly to particular models through the definition of  $\beta$  and  $\lambda$  parameters [27, 30].

Our potentials are defined as scalar perturbations of a flat, FRW metric

$$\begin{aligned} g_{00} &= -[1 + 2\Psi(\vec{x}, t)], \\ g_{ij} &= a^2(t) [1 - 2\Phi(\vec{x}, t)] \delta_{ij}, \end{aligned} \quad (4)$$

where we have made the conformal Newtonian gauge choice to fix the remaining two scalar degrees of freedom in the perturbed metric. In (4),  $\Psi$  is the Newtonian potential and is responsible for the acceleration of massive particles whereas  $\Phi$  is the curvature potential, which also contributes to the acceleration of relativistic particles.

We will consider a number of scenarios for the phenomenological modification to the standard gravitational force. We will assume that GR is valid up to a specified redshift. This is motivated by the stringent conditions set on any modifications to the standard paradigm by Big Bang Nucleosynthesis (BBN) observations of light element abundances in the early universe and of CMB anisotropies at recombination. Beyond the redshift where modifications take over we will assume either that the  $\mu$  and  $\eta$  parameters remain constant with a given value different from unity or that they follow a simple time-dependence.

This simple treatment raises two issues. Firstly, the time-dependence of the modification introduced in (2) is not motivated by any dynamical considerations and may not be self-consistent within the framework of the underlying theory responsible for the departure from GR. This is an unavoidable problem in the phenomenological approach taken here<sup>1</sup>. Secondly our prescription does not allow

for any spatial dependence of the modifications. This can be justified in part by requiring the simplest modifications however all mechanisms which generate deviations from GR will have to include some form of screening or cut-off mechanism, at the very least, acting on scales close to solar system and below in order to satisfy laboratory and solar system scale tests of GR. Indeed, all mechanisms proposed so far have some form of explicit screening mechanism acting either universal or environment dependent length scales. For the purpose of this exercise we shall omit any screening mechanism, effectively assuming it acts on scales smaller than any probed by the observations included in this work. However if the screening scale is effective at even moderate comoving scales of a few Mpc then we would expect some sensitivity of our results to this assumption, particularly where we have included cluster counts. We leave for future work the determination of the effect of scale dependent modifications on cluster count predictions which necessarily require the study of modified N-body simulations [33]. In this work we will restrict ourselves to elucidating the utility, or otherwise, of including cluster counts in combined constraints on MGPs.

The background expansion history is already constrained to be close to that of a  $\Lambda$ CDM model, we will therefore assume that the modified gravity mimics the expansion history of a standard  $\Lambda$ CDM setup. Having made this choice we are then left with probes of inhomogeneity as observables that could constrain any modifications. Throughout this work we take a fiducial  $\Lambda$ CDM cosmology described by the following parameters: The dimensionless Hubble rate in units of  $100 \text{ Km s}^{-1} \text{ Mpc}^{-1}$ ,  $h = 0.71$ , the density of matter (baryons + dark matter) and dark energy in units of the critical energy density,  $\Omega_m = 0.265$ , and  $\Omega_\Lambda = 0.735$  respectively, the optical depth to recombination  $\tau = 0.088$ , the amplitude of primordial, super horizon curvature perturbations  $\log(10^{10} A_s) = 3.071$  at  $k = 0.05 h \text{ Mpc}^{-1}$  and their spectral index  $n_s = 0.963$ . These parameters correspond to the WMAP 7-year best-fit parameters [34]. This model yields a large scale structure normalisation of  $\sigma_8 = 0.804$  for the standard deviations of fluctuations on scales of  $8 h^{-1} \text{ Mpc}$ .

### III. OBSERVABLES

A number of authors have examined the use of combinations of observables for forecasting future constraints on MGPs [9, 12–19]. Combinations have included weak lensing, CMB, galaxy redshift surveys, peculiar velocity surveys and cluster counts. In this work we will examine the combination of CMB cross-correlated with weak lensing surveys and combined with cluster counts. We have made this choice of observables due to the inherent simplicity in their sensitivity to MGPs and the potential to unambiguously interpret the data. The CMB on largest scales will be sensitive to any modification of gravity through the ISW effect as probed by photons,

<sup>1</sup> However see [32] for recent work in defining self-consistent MGPs for expansions around GR.

whilst on the smaller scales will still provide uncorrelated constraints on the conventional parameters of the cosmological model. Weak lensing, being a relatively low-redshift sourced signal, will provide direct constraints on the MGPs, also, as probed by photons. The cross-correlation of the two observables will serve to enhance the sensitivity to the MGPs and to reduce the degeneracies between the MGPs and other parameters.

As with all probes of MGPs, a set of observables that depends on the growth of non-relativistic matter perturbations is required to constrain any difference between metric perturbations. For this investigation we have chosen to focus on cluster counts. These offer the prospect of an unbiased tracer of the dark matter distribution as opposed to measurements of galaxy redshift power spectra which are known to suffer from scale dependent biasing. To calculate the theoretical predictions from models of modified gravity we will employ the `CAMB sources`<sup>2</sup> package which has been modified to include modifications of gravity during the free streaming regime after recombination (`MGCAMB` [30]). The `CAMB sources` package allows the calculation of full-sky power spectra for a number of generic ‘sources’ which can be those of eg. weak lensing, 21cm emission, etc. A useful feature of the package is the capability of separating out the contribution to an individual source into redshift bins, a feature we will be making use of for our forecasted weak lensing surveys and cluster count predictions. All the models used assume a standard  $\Lambda$ CDM background and the effect of modified gravity is solely to change the evolution of perturbations around the background. Additionally, We use the matter power spectrum calculated by the code as an input for our calculation of the mass functions, which are integrated to give the expected cluster counts described below.

Throughout this Section and as we discuss our results we will refer to a number of ‘Stages’ of observations which summarise a time-line of future surveys in each category of observables discussed. The exact definition of the Stages considered will be discussed in Section IV after we introduce our three choices of observables in more detail.

### A. Cluster Counts

Galaxy clusters are some of the largest collapsed structures in the universe. According to the standard  $\Lambda$ CDM cosmology, they typically consist of hot gas bound in a large cold dark matter halo. Clusters have been looked at in the context of constraining dark energy [11, 35–40], and some of the studies looking at constraining  $\gamma$  or the MGPs [8, 11, 18, 41–44]. They are a useful cosmological probe as their size corresponds to scales near the linear

to non-linear transition in the underlying dark matter power spectrum. This has several consequences: they probe the tail of the matter perturbation spectrum and are therefore a sensitive probe of growth. In addition, galaxy cluster counts can be predicted accurately from linear theory, using semi-analytic formulae or formulae calibrated from N-body simulations. These prescriptions have been accurately calibrated using  $\Lambda$ CDM models but may need to be revisited if they are to be extended to modified dark energy or gravity models. The formulae that are calibrated by N-body simulations work over a range of cosmologies, but their suitability to perturbed dark energy and modified gravity cosmologies have not been investigated fully. Some specific dark energy models have been looked at [45, 46] as well as DGP [43, 44, 47] and  $f(R)$  [48]. In most cases the non-linear fitting functions and mass functions have been found to be sufficiently accurate [49]<sup>3</sup>.

As previously mentioned, we are not taking into account any physical screening mechanism in this work which would naturally lead to modifications to the mass function and any semi-analytical prediction of cluster counts. We will look into the impact of screening scales on the predictions in future work [33] and use the  $\Lambda$ CDM calibrated predictions for the forecasting exercise being carried out here.

The number of clusters observable over a fraction of the sky  $f_{\text{sky}}$  and with a redshift dependent mass resolution limit  $M_{\text{lim}}(z)$  in a redshift bin spanning the interval  $z$  to  $z + \Delta z$  can be calculated by integrating the comoving number density  $dn/dM$  of objects with mass  $M$

$$N_{\Delta z} = 4\pi f_{\text{sky}} \int_z^{z+\Delta z} dz' \frac{dV}{dz' d\Omega} \int_{M_{\text{lim}}(z')}^{\infty} \frac{dn}{dM} dM, \quad (5)$$

where  $dV/dz d\Omega = r^2(z)/H(z)$  is the comoving volume at redshift  $z$  in a flat universe, with  $H(z)$  the Hubble rate and  $r(z) = \int_0^z dz'/H(z')$  is the comoving distance to that redshift.

Much work has gone into predicting the shape of the mass function  $dn/dM$  for a given linear power spectrum starting with the semi-analytical Press-Schechter formalism given by the mass function

$$\frac{dn}{dM} = -\sqrt{\frac{2}{\pi}} \frac{\rho}{M} \frac{d\sigma_M}{dM} \frac{\delta_c}{\sigma_M^2} \exp\left[-\frac{1}{2} \frac{\delta_c^2}{\sigma_M^2}\right], \quad (6)$$

where  $\rho$  is the background density of dark matter today,  $\delta_c = 1.686$  is a critical density contrast and  $\sigma_M^2$  is the variance of the dark matter fluctuations in a sphere of radius  $R = (3M/4\pi\rho)^{1/3}$  defined by the integral of the linear matter power spectrum  $P(k)$  over wavenumber  $k$

$$\sigma_M^2 = \frac{1}{2\pi^2} \int_0^{\infty} W^2(kR) P(k) k^2 dk, \quad (7)$$

<sup>2</sup> <http://camb.info/sources/>

<sup>3</sup> See also [41] for references regarding testing the fitting function from [50]

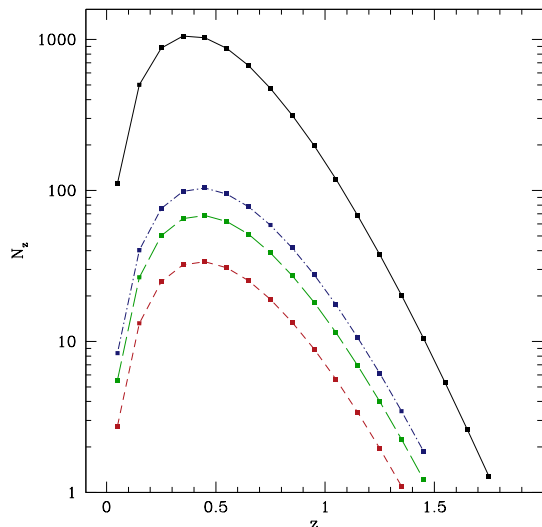


FIG. 1: Cluster counts in 20 redshift bins for the fiducial  $\Lambda$ CDM model calculated using (9) with redshift independent  $M_{\text{lim}} = 5.0 \times 10^{14} M_{\odot}$ , solid (black). We also show the difference in expected counts for models with  $\mu = 1.0023$  (short-dashed, red), 1.0046 (long-dashed, green), and 1.0069 (dash-dotted, blue) corresponding to 1, 2, and 3 $\sigma$  deviations from GR for our Stage I forecasted constraints (see Section V).

with top-hat filter function

$$W(kR) = 3 \left( \frac{\sin(kR)}{(kR)^3} - \frac{\cos(kR)}{(kR)^2} \right). \quad (8)$$

Successive studies have yielded formulae of increasing complexity and accuracy [51–55], particularly for cluster predictions. Other approaches have used N-body calibrated empirical formulae for the mass function. In this work we adopt the results of [50] where the mass function is expressed as

$$\frac{dn}{dM} = -0.316 \frac{\rho}{M} \frac{d\sigma_M}{dM} \frac{1}{\sigma_M} \exp[-|0.67 - \log(\sigma_M)|^{3.82}]. \quad (9)$$

Since we keep an expansion history that is consistent with  $\Lambda$ CDM, the effect of the modified gravity parameters will be to change the growth history and hence the matter power spectrum. The linear matter power spectrum is calculated at the desired redshifts by the `MGCAMB` code, and this is then fed into the mass function (9) and cluster abundance (5).

As can be seen in (9), the number of clusters is exponentially sensitive to the amount of growth that has occurred, and should therefore provide a strong constraint on the  $\mu$  parameter. This sensitivity can be seen in Figure 1, where we show the expected cluster counts in redshift bins of width  $\Delta z = 0.1$  for a Planck-like experiment observing 70% of the sky. The curve was obtained from (9) assuming a constant limiting mass

$M_{\text{lim}} = 5.0 \times 10^{14} M_{\odot}$ , consistent with what is expected of Planck [20]. We also show the increase in cluster counts expected for the same observational setup with  $\mu = 1.0023$ , 1.0046 and 1.0069 corresponding to 1, 2, and 3 $\sigma$  deviations from GR for our Stage I forecasted constraints (see Section V). These values represent a departure from the GR value of  $\mu$  of less than 1%, however they lead to an increase of between 5 and 10% in the number of observed clusters.

Our theoretical predictions for the number of clusters in redshift bins will be compared to predicted SZ catalogues for a number of future observational stages. The SZ effect [56] is a nearly redshift independent tracer of clusters that is due to the re-scattering of CMB photons by hot intracluster gas. The observational limits on SZ observations are, in principle, determined simply by resolution and sky coverage. The frequency dependence of the effect also makes it possible to cleanly identify clusters in any multi-frequency CMB observations spanning the null frequency of  $\sim 220$ GHz where the effect changes sign. An additional advantage of SZ surveys over X-ray surveys of clusters is that the effect is less sensitive to the internal structure of the cluster than X-ray emission and this should make it easier to obtain unbiased estimates of the cluster masses [39, 57].

In principle, the limiting mass for an SZ survey is a redshift dependent quantity. The source of this is the change of apparent size of the cluster with redshift; the actual distortion to the temperature has no redshift dependence. We calculated the effect that the full redshift dependent limiting mass had on the constraints (see Appendix A). Since the effect of the redshift dependent limiting mass on the constraints turns out to be negligible, we have used a constant, redshift independent limiting mass for all our forecasts.

The exponential sensitivity of cluster counts to the amplitude of the underlying density perturbations introduces some issues of accuracy. The mass of a given cluster must necessarily be estimated from some proxy signal such as X-ray temperature or SZ flux. Use of cluster counts to constrain model parameters is therefore subject to any bias introduced in the determination of the cluster mass from the available information. Any forecasts that do not take this uncertainty into account may potentially underestimate the errors in model parameters.

Following [58], we consider the probability of assigning a mass  $\tilde{M}$  to a cluster of true mass  $M$  to be given by a Gaussian distribution in the logarithm of  $M$

$$P(\tilde{M}|M)d\tilde{M} = \frac{1}{\sqrt{2}\sigma_{\mathcal{M}}} \exp\left[-\frac{1}{2} \frac{(\tilde{\mathcal{M}} - \mathcal{M})^2}{\sigma_{\mathcal{M}}^2}\right] d\tilde{M}, \quad (10)$$

where  $\mathcal{M} = \ln M$  and  $\tilde{\mathcal{M}} = \ln \tilde{M}$ . In defining the distribution we have assumed there is no systematic bias in the estimates of the cluster masses, only a scatter induced by the uncertainty. The scatter is parametrised by the standard deviation of the distribution  $\sigma_{\mathcal{M}}$ .

We can now calculate the expected comoving number

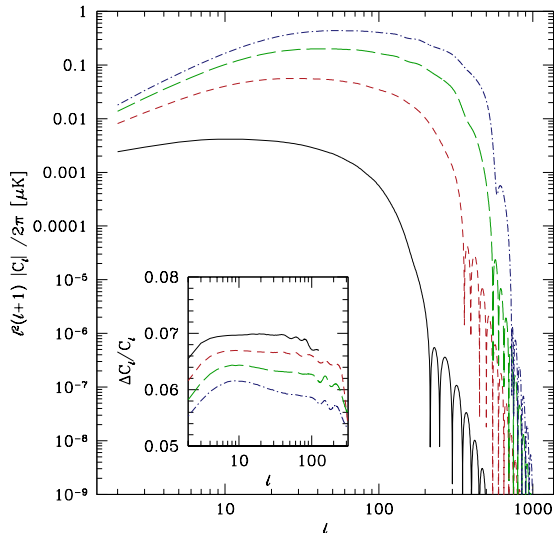


FIG. 2: The cross-correlation signal between CMB temperature and weak lensing convergence from Stage I type survey combination (see Table I) as a function of angular multipole  $\ell$ . The curves shown are for the fiducial  $\Lambda$ CDM model. The cross-correlation is shown in four redshift bins with amplitude increasing with redshift. The inset shows the fractional change in the cross-correlation signal with MGP values  $\eta = 1.03$  and  $\mu = 1.008$  corresponding to a  $1\sigma$  shift given our final constraints (see Section V).

density given the distribution in estimated masses with observational cutoff  $\widetilde{M}_{\text{lim}}$

$$n(\sigma_{\mathcal{M}}) = \int_{\widetilde{M}_{\text{lim}}}^{\infty} \frac{d\widetilde{M}}{\widetilde{M}} \int_0^{\infty} dM \frac{dn}{dM} P(\widetilde{M}|M). \quad (11)$$

Substituting in the expression for the probability and carrying out the integral yields

$$n(\sigma_{\mathcal{M}}) = \frac{1}{2} \int_0^{\infty} dM \frac{dn}{dM} \text{erfc} \left[ \frac{1}{\sqrt{2}} \frac{(\widetilde{M}_{\text{lim}} - M)}{\sigma_{\mathcal{M}}} \right]. \quad (12)$$

Integrating the density over redshifts gives a modified number count as a function of the uncertainty  $\sigma_{\mathcal{M}}$

$$N_{\Delta z}(\sigma_{\mathcal{M}}) = 4\pi f_{\text{sky}} \int_z^{z+\Delta z} dz' n(\sigma_{\mathcal{M}}) \frac{dV}{dz' d\Omega}, \quad (13)$$

This can be used in our forecasts to account for the uncertainty. We will adopt a reference value of  $\sigma_{\mathcal{M}} = 0.25$  [58]. We will include the  $\sigma_{\mathcal{M}}$  as an extra parameter in the Fisher matrices for the cluster counts and marginalise it out by eliminating its contribution to the inverse Fisher matrix.

## B. CMB

With the release of Planck satellite results only a few years away we are entering an era where observations of the CMB total intensity spectrum will have reached the sample variance limit throughout scales where primary effects dominate the signal. As such, in all of our forecasts, we will be assuming a Planck-like observation of the CMB angular power spectrum out to multipoles  $\ell = 2000$ .

The sensitivity to MGPs in the CMB spectrum is restricted to the largest scales. This is due the constraint that gravity is not modified at early times and through recombination. This means anisotropies generated through the Sachs Wolfe effect on super-horizon scales and acoustic effects on sub-horizon scales at recombination will not be affected by our late time modifications. The only signal will arise on the largest scales due to the ISW effect which is sourced as the Universe transitions into a dark energy dominated model and the potential starts to decay. The effect can be described by the integral of the time-derivative of the sum of metric potentials along the line of sight as photons free stream after recombination

$$\left( \frac{\delta T}{T} \right)_{\ell} = - \int_0^{\tau_0} e^{-\theta(\tau)} \frac{\partial}{\partial \tau} [\Phi(1 + \eta)] j_{\ell}[k(\tau - \tau_0)] d\tau, \quad (14)$$

where  $(\delta T/T)_{\ell}$  is the multipole expanded, fourier transform of the CMB temperature fluctuation at conformal time today,  $\tau_0$ ,  $\theta$  is the optical depth, and the spherical Bessel functions  $j_{\ell}$  describe the projection of plane-wave modes on the celestial sphere. The ISW contributes to the power on the largest scales as it is only sourced at late times (we will disregard any effect from the early ISW effect due to potential evolution close to the radiation to matter transition). These modes are fundamentally ill-sampled due to the small number of  $a_{\ell m}$  coefficients on these scales and also suffer degeneracy with other effects such as the Sachs Wolfe signal from last scattering and the effect of reionisation. One way to gain further constraining power from such a sample variance limited signal is to cross-correlate the CMB with other large scale observables, indeed, low-significance detections of a dark energy component have been reported via cross-correlation with a number of tracer of large scale structure [59–67]. We will also take advantage of this by cross-correlating with template weak lensing surveys.

As our template CMB observable we take an angular power spectrum  $C_{\ell}$  from the best-fit  $\Lambda$ CDM model and add sample and noise variance according to a Planck-like survey covering an area corresponding to 70% of the sky. The error at each multipole can be calculated from the observational parameters via

$$\delta C_{\ell} = \sqrt{\frac{2}{f_{\text{sky}}(2\ell + 1)}} (C_{\ell} + N_{\ell}), \quad (15)$$

where  $N_{\ell}$  is a function of resolution ( $\theta$ ), the number of de-

tectors ( $N_{\text{det}}$ ) and Noise Equivalent Temperature ( $T_{\text{NET}}$ ) in a given channel, as well as the overall integration time ( $t_{\text{tot}}$ )

$$N_{\ell} = \left[ \frac{1}{(\sigma\theta)^2} \exp\left(-\frac{\ell(\ell+1)\theta}{8 \ln 2}\right) \right]^{-1}, \quad (16)$$

with  $\sigma$  evaluated as

$$\sigma = \frac{4\pi f_{\text{sky}}}{\theta} \frac{T_{\text{NET}}}{\sqrt{N_{\text{det}} t_{\text{tot}}}}. \quad (17)$$

For our Planck-like survey, we will use the values  $\theta = 7.1$  arcminutes,  $N_{\text{det}} = 32$ ,  $T_{\text{NET}} = 62.0 \mu\text{K s}^{1/2}$ ,  $f_{\text{sky}} = 0.7$  and  $t_{\text{tot}} = 14$  months.

### C. Weak lensing

The third observable we will use is the convergence power spectrum from weak lensing surveys. Weak lensing is a relatively new cosmological tool and is a measure of the small distortions of background galaxies due to gravitational lensing by large scale structure [68]. Distortions of individual background galaxies are virtually impossible to measure due to the intrinsic ellipticity of galaxies. However, statistical results averaging over large numbers of galaxies are now routinely reported [69]. The convergence  $\kappa$  is a measure of the Laplacian of the potentials responsible for the lensing along the line of sight and can be calculated as an integral over the comoving radial distance  $r$  as

$$\kappa = \frac{k^2}{2} \int_0^{r_{\infty}} \Phi(1 + \eta) g(r) dr, \quad (18)$$

where we have expressed quantities in the Fourier domain and  $g(r)$  is a filter function determined by the redshift distribution of background galaxies being lensed  $w[r(z)]$

$$g(r) = r \int_0^{r_{\infty}} \left[ 1 - \frac{r'}{r} \right] w(r') dr'. \quad (19)$$

The convergence power spectra can be calculated using **MGCAMB** for the modified gravity case and can be split into contributions from separate redshift bins assuming the observations are able to obtain sufficiently accurate photometric redshifts of the background sources. In all cases we will include multipoles  $\ell \leq 2000$  to avoid complications that arise due to lensing from non-linear scales. For our initial weak lensing survey, we consider a DES-like survey. DES is a ground based survey at the Cerro-Tololo Inter-American Observatory in Chile that is scheduled to begin observations in 2011. It will survey 5000 sq deg over 5 years and aims to constrain dark energy with 4 probes: supernovae, BAO, galaxy clusters and weak lensing, the latter being the probe we are interested in here. We consider 4 redshift bins between  $z = 0$  and  $z = 2$ , following the prescription in [12].

TABLE I: Parameters used for the three Stages of future observations used in our forecasts.

	$f_{\text{sky}}^{\kappa}$	$N_g$	$f_{\text{sky}}^{\text{SZ}}$	$M_{\text{lim}} (M_{\odot})$
Stage I	0.121	$2.14 \times 10^8$	0.7	$5.0 \times 10^{14}$
Stage II	0.485	$3.6 \times 10^8$	0.7	$2.5 \times 10^{14}$
Stage III	0.485	$2.88 \times 10^9$	0.7	$1.0 \times 10^{14}$

One of the biggest sources of error in these surveys will be errors in the photometric determination of redshifts of the background galaxies. We model the overall redshift distribution of the sources as

$$w(z) = N_g \frac{4}{\sqrt{\pi}} \frac{z^2}{z_{\star}^3} \exp\left[-\frac{z^2}{z_{\star}^2}\right], \quad (20)$$

such that  $\int w(z) dz = N_g$ , the total number of background galaxies and  $z_{\star}$  defines the median redshift of the distribution. We take a reference value of  $z_{\star} = 0.46$  for our template weak lensing surveys.

We can take into account the uncertainty in photometric redshifts when breaking down the signal into contributions from different redshift bins. We define four, overlapping distributions  $w_i(z)$  with  $i = 1, 2, 3$ , and 4 with the constraint

$$w(z) = \sum_{i=1}^4 w_i(z), \quad (21)$$

with

$$w_i(z) = \frac{1}{2} w(z) \left[ \text{erfc}\left(\frac{z_{i-1} - z}{\sqrt{2} \sigma(z)}\right) - \text{erfc}\left(\frac{z_i - z}{\sqrt{2} \sigma(z)}\right) \right]. \quad (22)$$

The bins are centred at redshifts  $z_i$  corresponding to 0.1, 0.5, 0.9, and 1.3, as shown in Figure 3, with the photometric redshift error given by  $\sigma = 0.05(1 + z)$ .

We can model the statistical error in the angular power spectrum of the convergence from each redshift bin as a sum of sample and noise contributions

$$\delta C_{\ell}^{\kappa_i} = \sqrt{\frac{2}{f_{\text{sky}}(2\ell + 1)}} \left( C_{\ell}^{\kappa_i} + \frac{\langle \gamma^2 \rangle}{N_g^i} \right), \quad (23)$$

where  $\langle \gamma^2 \rangle$  is the variance of the intrinsic ellipticity of a typical galaxy in the survey and  $N_g^i = \int w_i(z) dz$  is the number of galaxies in each redshift bin. See table I for the parameters used to model the three Stages of weak lensing experiments. In all cases  $\langle \gamma^2 \rangle = 0.16$  and the photometric redshift error is given by  $\sigma = 0.05(1 + z)$ .

With the advent of large scale weak lensing surveys the possibility of cross-correlating CMB and convergence maps will become a reality. This will make use of all the available information in the data since the signal in two such maps will be correlated. The cross-correlation will be most useful in this case since dependence on MGPs



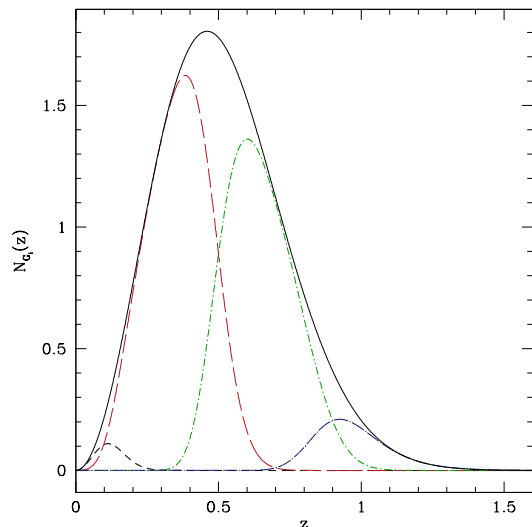


FIG. 3: Total redshift distribution of the sources (solid line) and redshift coverage of the four weak lensing bins used for forecasting the weak lensing experiments. In calculating the redshift coverage of the bins, we have marginalised over the uncertainty in determining the redshift of the sources.

is expected to be strongest on the largest scales. In Figure 2 we show the expected cross-correlation signal between CMB and the four weak lensing survey redshift bins used in our analysis. The inset shows the fractional change in the cross-correlation induced by a change in MGPs from their fiducial GR values to  $\eta = 1.03$  and  $\mu = 1.008$ . These correspond to  $1\sigma$  deviations from the fiducial values given our forecasted constraint obtained from CMB and weak lensing data alone (see Section V).

#### IV. FORECASTS

In this Section we carry out forecasts for a number of future observational ‘Stages’. Since the Planck satellite will provide a sample variance limited map of CMB total intensity anisotropies covering angular scales where the signal of interest lies we will use our Planck-like setup as the CMB contribution throughout. For weak lensing and cluster counts we will assume three distinct observational stages corresponding to short, medium, and long-term development of survey sizes and accuracies.

- **Stage I:** Corresponds to a Planck-like cluster survey and a DES (Dark Energy Survey)-like weak lensing survey. DES is being carried out on the Cerro Tololo Inter-American Observatory in the Chilean Andes and should start taking data in late 2011. DES is modelled with a total of 214 million galaxies over 12% of the sky.

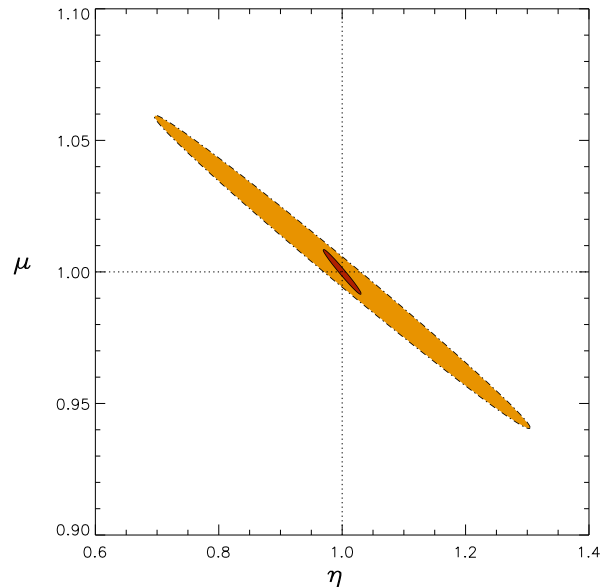


FIG. 4: Fisher constraints on  $\eta$  and  $\mu$  from the combination of Stage I CMB and weak lensing observations with and without cross-correlation (green/dot-dashed ellipse and red/solid ellipse respectively).

- **Stage II:** This stage includes a weak lensing survey based on PANSTARRS and as such is modelled with a total of 360 million galaxies over 48.5% of the sky. The SZ survey is modelled by keeping the same  $f_{\text{sky}}$  as with Planck, but lowering the limiting mass to  $2.5 \times 10^{14} M_{\odot}$ . This corresponds to lowering the smallest change in flux that the SZ survey can detect.
- **Stage III:** This includes a weak lensing survey based on the LSST, due to begin taking data in 2020. This survey is modelled with the same fraction of the sky as PANSTARRS (48.5%), but with a total number of galaxies of 2880 million. The third stage SZ survey assumes a limiting mass of  $1.0 \times 10^{14} M_{\odot}$ .

The sampling characteristics for the three Stages are summarised in Table I. We have kept the same intrinsic ellipticity, redshift bins and photometric errors assumptions for all Stages as it is unclear how photometric redshift resolution will evolve as surveys increase in size and complexity.

Our forecasts are based on Fisher matrix estimates of errors in a subset of parameters that comprises the MGPs,  $\eta$  and  $\mu$ , and the two parameters from the standard model that are expected to be most correlated with them, the total matter density  $\Omega_m$  and the primordial amplitude of scalar curvature perturbations  $A$ . In varying only these four parameters we are assuming that the remaining four standard  $\Lambda$ CDM parameters are well constrained by sig-



Parameter	Stage I		Stage II		Stage III	
	CMB $\otimes$ WL	CMB $\otimes$ WL + CC	CMB $\otimes$ WL	CMB $\otimes$ WL + CC	CMB $\otimes$ WL	CMB $\otimes$ WL + CC
$\Delta\eta$	$3.0 \times 10^{-2}$	$5.5 \times 10^{-3}(1.5 \times 10^{-2})$	$1.8 \times 10^{-2}$	$4.4 \times 10^{-3}(8.8 \times 10^{-3})$	$1.5 \times 10^{-2}$	$2.4 \times 10^{-3}(5.5 \times 10^{-3})$
$\Delta\mu$	$8.4 \times 10^{-3}$	$2.3 \times 10^{-3}(4.5 \times 10^{-3})$	$5.5 \times 10^{-3}$	$2.1 \times 10^{-3}(3.1 \times 10^{-3})$	$4.8 \times 10^{-3}$	$1.5 \times 10^{-3}(2.1 \times 10^{-3})$

TABLE II: Fisher errors on  $\eta$  and  $\mu$  for Stage I, II, and III observations for different combinations of observables: cross-correlation of CMB and weak lensing (CMB  $\otimes$  WL) and addition cluster counts (CC). The values in brackets show how the errors are affected by the marginalisation over a mass assignment error.

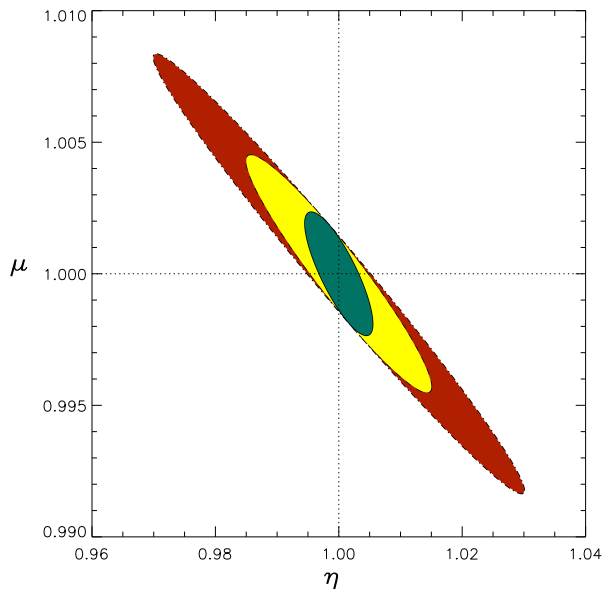


FIG. 5: Fisher constraints on  $\eta$  and  $\mu$  from cross-correlated CMB and weak lensing measurements (Stage I) are shown by the red area (dot-dashed contour). The improvement obtained by adding Stage I cluster counts is seen in the green area (solid contour). The outer ellipse corresponds to the inner ellipse of Fig. 4. Adding an uncertainty in the mass assignment for the clusters of  $\sigma_{\mathcal{M}} = 0.25$  decreases the impact of adding cluster data as shown by the yellow (dashed) ellipse.

nals orthogonal to those being used in our analysis. A combination of high resolution CMB spectra, including polarisation  $E$ -modes, and a standard prior on the value of the Hubble rate will ensure most of the remaining parameters are fixed to within a few percent of their nominal values, which should have a minimal impact on the four parameters being considered in this work.

An alternative to our Fisher matrix based method would be to Monte Carlo Markov Chain (MCMC) sample the joint posterior distribution of our parameter set by evaluating the likelihood explicitly. However this would involve the definition of a likelihood as a function of realisations of the observables (and their cross-correlation) and the added complexity is not warranted for this kind of exercise at this stage.

It should be noted that use of a Fisher matrix to estimate parameter errors assumes that the observables are distributed as Gaussian variates. This is not true in all cases considered here since we are considering power spectra and number counts but as long as the true answer lies close to our fiducial values for the four parameters the errors should give a good indication of the constraints. Given a set of  $n$ , uncorrelated measurements  $C_a$ , with  $a = 1, \dots, n$  and measurement errors  $\delta C_a$ , the Fisher matrix for a set of  $m$  parameters  $\lambda_\alpha$  with  $\alpha = 1, \dots, m$ , can be evaluated as

$$F_{\alpha\beta} = \sum_{a=1}^n \frac{1}{\delta C_a} \frac{\partial C_a}{\partial \lambda_\alpha} \frac{\partial C_a}{\partial \lambda_\beta} \frac{1}{\delta C_a}, \quad (24)$$

where  $\beta = 1, \dots, m$ .

The Fisher matrix represents the ensemble average of the negative curvature in the log likelihood of the model parameters and its inverse, in this limit, is therefore the covariance matrix in those parameters. The Fisher matrix is simple to evaluate since it involves only the first derivatives of the signal with respect to the model parameters. These can be evaluated either analytically or numerically. Here we use a central difference scheme to numerically approximate the derivatives to second order in the step-size. The central difference is sampled by evaluating the models with given step-sizes either side of the fiducial model in all parameter directions.

For the cluster counts case the measurement consists of counts in each of twenty redshift bins  $N_i$ , as shown in Figure 1 for the fiducial model, and the Fisher matrix is calculated as

$$F_{\alpha\beta} = \sum_{i=1}^{20} \frac{1}{\sigma_{N_i}^2} \frac{\partial N_i}{\partial \lambda_\alpha} \frac{\partial N_i}{\partial \lambda_\beta}, \quad (25)$$

where we have assumed a shot noise model for the error in the counts.

Fisher matrices from independent data can be added and then inverted to obtain error estimates for the combination of data. Since we will rely heavily on the cross-correlation of CMB and weak lensing measurements to extract the relevant signal we calculate the combined Fisher matrix for this cross-correlation to add to (25). The Fisher matrix formalism can be easily extended to the correlated measurement case. We treat the combination of CMB and weak lensing measurements at a given multipole  $\ell$  as a matrix,  $\mathbf{C}_\ell$ , of angular, cross-correlation

power spectra with dimension  $n \times n$ . In our case the index  $n$  spans both CMB and convergence angular power spectrum measurements (over the four redshift bins) i.e.  $T, \kappa_1, \kappa_2, \kappa_3, \kappa_4$  with the symmetric form

$$\mathbf{C}_\ell \equiv \begin{pmatrix} C_\ell^{TT} & C_\ell^{T\kappa_1} & C_\ell^{T\kappa_2} & \dots \\ \cdot & C_\ell^{\kappa_1\kappa_1} & C_\ell^{\kappa_1\kappa_2} & \dots \\ \cdot & \cdot & C_\ell^{\kappa_2\kappa_2} & \dots \\ \cdot & \cdot & \cdot & \dots \end{pmatrix}. \quad (26)$$

Each measurement matrix will have a corresponding covariance matrix with non-zero off-diagonal contributions due to the correlations in the signal part of the measurements whilst the diagonals will have contributions from both signal and noise

$$\Sigma_\ell \equiv \begin{pmatrix} (\delta C_\ell^{TT})^2 & (\delta C_\ell^{T\kappa_1})^2 & (\delta C_\ell^{T\kappa_2})^2 & \dots \\ \cdot & (\delta C_\ell^{\kappa_1\kappa_1})^2 & (\delta C_\ell^{\kappa_1\kappa_2})^2 & \dots \\ \cdot & \cdot & (\delta C_\ell^{\kappa_2\kappa_2})^2 & \dots \\ \cdot & \cdot & \cdot & \dots \end{pmatrix}, \quad (27)$$

where the diagonal elements correspond to the square of standard deviations (15) and (23) and the off-diagonal terms can be evaluated using

$$(\delta C_\ell^{XY})^2 = \frac{1}{(2\ell + 1)} \left[ \frac{C_\ell^{XX} C_\ell^{YY}}{\sqrt{f_{\text{sky}}^X f_{\text{sky}}^Y}} + \frac{(C_\ell^{XY})^2}{\min(f_{\text{sky}}^X, f_{\text{sky}}^Y)} \right]. \quad (28)$$

Here  $C_\ell^{XY}$  is the model cross-correlation power spectrum for the two observables which is also computed by **CAMB sources**.

The Fisher matrix for this generalised case can be evaluated as

$$F_{\alpha\beta} = \sum_\ell \text{Tr} \left[ \frac{\partial \mathbf{C}_\ell}{\partial \alpha} \cdot \Sigma_\ell^{-1} \cdot \frac{\partial \mathbf{C}_\ell}{\partial \beta} \right]. \quad (29)$$

A further contribution to the Fisher matrix is given by the sample variance depending on the parameters

$$F_{\alpha\beta} = \frac{1}{2} \sum_\ell \text{Tr} \left[ \frac{\partial \Sigma_\ell}{\partial \alpha} \cdot \Sigma_\ell^{-1} \cdot \frac{\partial \Sigma_\ell}{\partial \beta} \cdot \Sigma_\ell^{-1} \right]. \quad (30)$$

This term is sub-dominant to the first, however we have included it in the analysis for the sake of completeness.

## V. RESULTS

We initially considered the case where the MGPs switch from their fiducial, GR value to a new, time independent value, at a fixed redshift,  $z_{\text{mg}}$ . There is a wide range in redshifts, spanning from the time of recombination to the end of the so called ‘dark-ages’, where modifications to GR could come into effect. Here we chose  $z_{\text{mg}} = 30$  for the time-independent case which ensures that most non-linear structures observed formed in the presence of

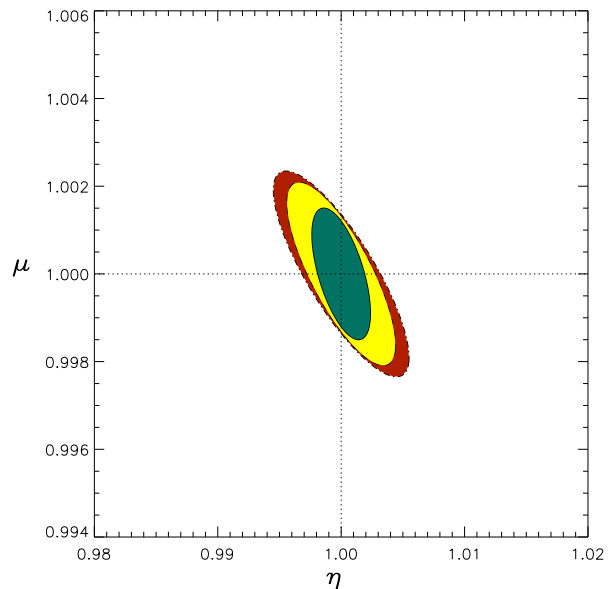


FIG. 6: Fisher constraints on  $\eta$  and  $\mu$  from the combination of CMB, weak lensing, and cluster counts for the three observational stages. Stage I, red (dot-dashed); Stage II, yellow (dashed); Stage III, green (solid).

the modifications. We also consider the case where the MGPs have a simple, linear redshift dependence between their GR values at  $z_{\text{mg}}$  and their late time values  $\eta_0$  and  $\mu_0$  at  $z = 0$ . Specifically we show how our results change for a choice  $z_{\text{mg}} = 3$  and  $z_{\text{mg}} = 1$ .

The CMB is most effective in constraining the standard parameters of the concordance model of cosmology. The only effect of the MGPs is on the ISW effect, and this has several shortcomings. The increase of power due to the MGPs is not large, and this is compounded by the higher cosmic variance on these scales. The uncertainties in weak lensing mostly come down to a degeneracy between  $\eta$  and  $A$ . This, is why, when combining CMB and Weak lensing observations, the constraints on the modified gravity parameters improve significantly. The extra information obtained from cross correlating the two observations emphasises this complementarity of the two sets of data. Figure 4 shows how the constraints on  $\eta$  and  $\mu$  improve when the cross-correlation between CMB and weak lensing is included in the Fisher estimates. The contours shown the  $1-\sigma$  constraints obtained from the inverse of the Fisher matrix for all four parameters. We ensure our final errors account for marginalisation over our nuisance parameters  $\Omega_m$  and  $\ln A$  by only ignoring the matrix elements corresponding to these parameters after inverting the full Fisher matrix.

Even after taking into account the cross-correlation between CMB and weak lensing a significant degeneracy in  $\eta$  remains due to the correlation between the two gravitational potentials in both signals. Adding cluster counts

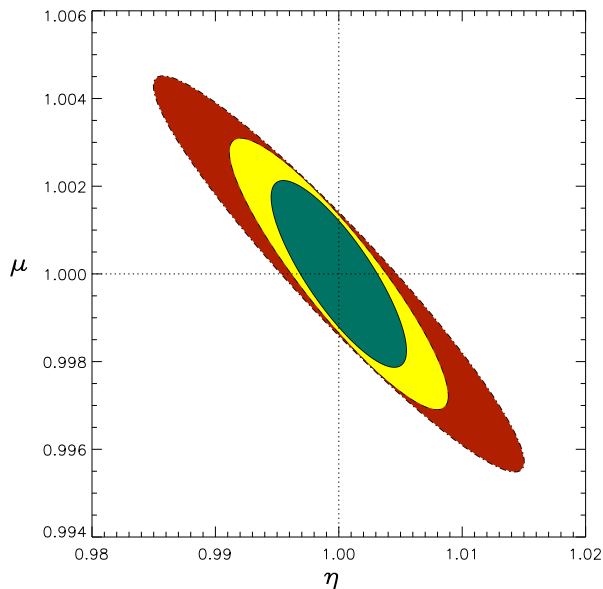


FIG. 7: Same as in Fig. 6 but with a mass assignment uncertainty of  $\sigma_{\mathcal{M}} = 0.25$  included in the constraints.

to the mix improves the situation since their signal is highly sensitive to just  $\Psi$  and therefore to the parameter  $\mu$ , which affects the growth rate of structure. This also has a large effect on the  $\eta$  parameter as the addition breaks the remaining correlations and allows the CMB and weak lensing observations to constrain  $\eta$ . The effect of adding Stage I cluster counts is shown in Figure 5. As mentioned earlier, there are some uncertainties associated with cluster counts. As can be seen readily from Figure 5, although marginalising over these uncertainties reduces the impact of clusters, they still add to the constraining power of the CMB and Weak lensing.

The comparison for Stage I, II, and III Fisher results in  $\eta$  and  $\mu$  are shown in Figure 6. The effect of adding a marginalisation over the mass assignment uncertainty is shown in Figure 7. The constraints worsen by a factor of between 2 and 3 when the uncertainty is taken into account but we stress that our estimates are conservative since we have not allowed for any improvement in  $\sigma_{\mathcal{M}}$  in successive Stages.

A summary of the results is shown in Table II for all three Stages. The forecasted errors  $\Delta\eta$  and  $\Delta\mu$  are shown with and without addition of cluster counts (CC). All constraints use the cross-correlation signal between CMB and weak lensing ( $\text{CMB} \otimes \text{WL}$ ) and the values in brackets show the effect of adding in the mass assignment uncertainty to the cluster counts.

In general, we find that the MGPs can be constrained to within a few percent using our forecasted surveys. The  $\mu$  parameter is most constrained by the observations. This is not surprising since it is the parameter that affects the growth history directly. Including the mass assignment

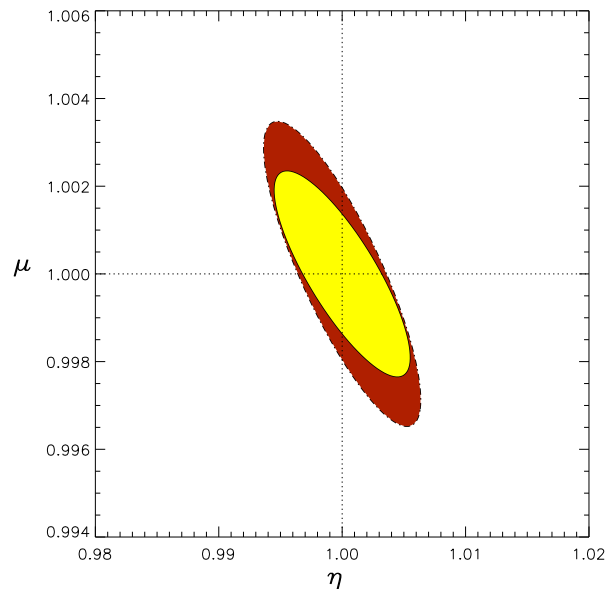


FIG. 8: Fisher constraints on  $\eta$  and  $\mu$  from the combined CMB, weak lensing, and cluster counts for the time-independent (solid/yellow) and time-dependent (dot-dashed/red) modified gravity parameters. In both cases  $z_{\text{mg}} = 30$  but for the latter a linear redshift-dependence is assumed (31).

error in the cluster counts reduces the constraints by approximately a factor of 2. The improvement obtained from successive Stages is limited, however the Stages recover the constraining power that was lost to the mass assignment error of the cluster counts. This reinforces the need for increased sensitivity and survey size for future observations as it hedges against systematic effects such as mass and photometric redshift resolution taken into account here.

To gauge the robustness of our predictions with respect to our choice of fixed  $\eta$  and  $\mu$ , we add a linear time dependence in the MGPs of the form

$$\mu(z) = (\mu_0 - 1) \left( \frac{z_{\text{mg}} - z}{z_{\text{mg}}} \right) + 1, \quad (31)$$

with a similar expression for  $\eta$ . Here,  $\mu_0$  or  $\eta_0$  is the value of the MGP today ( $z = 0$ ), which is the parameter that will be constrained in the Fisher matrix analysis. As such, the choice of  $z_{\text{mg}}$ , which is not included as a parameter in the Fisher analysis, fixes the gradient of the linear time dependence. We are therefore testing our results with respect to a choice of  $z_{\text{mg}}$  rather than extending the parameter space to include a parametrised time dependence.

As before,  $z_{\text{mg}}$  is the redshift at which the modification to gravity ‘switches on’. As shown in Figure 8, allowing for this simple time dependence in the MGPs does not have a large impact on constraints for the case where

$z_{\text{mg}} = 30$ . Although the time dependence reduces the impact of the MGPs on the observations for the same value of the MGPs today, the relative effect is also different in each of the signals and leads to a small change in degeneracies. An additional signal is sourced in this case since the time dependence of  $\eta$  will affect the late-time ISW. These combination of effects partly cancel, which results in a small effect on the final constraints. It should be stressed that there are many different choices of time dependence for the MGPs and (31) is only one of these. In principle some other form of time dependence could lead to much larger effects in this type of comparison. A theoretically motivated form for the time dependence would be better justified, however, this would build in a model dependence which we are explicitly avoiding in this work.

Our results for  $z_{\text{mg}} = 30, 3, \text{ and } 1$  are summarised in Table III which can be compared to the Stage I results of Table II. We find the effect becomes large only at relatively low redshifts with the choice of  $z_{\text{mg}} = 1$  leading to an order of magnitude increase in Fisher errors. This result is not indicative of the ability of the observations to constrain any possible time behaviour of the modified gravity theory but rather it illustrates the sensitivity of the observables to the departure from GR integrated over time.

## VI. DISCUSSION

Future generations of large area surveys hold much promise in testing the validity of GR. In this work we have examined the impact, on MGP constraints, of future cosmic shear and cluster count data used in combination with CMB measurement. We have found that this combination can constrain the MGPs to sub-percent accuracy. In particular the inclusion of cluster counts, which are highly sensitive to any change in the growth of the matter perturbations, adds a strong refinement in the search for any deviations from the standard GR values of the MGPs. However we have also shown that the inclusion of a simple model for calibration uncertainties in the counts can affect the errors.

There are, of course, other observables that can constrain the growth of matter perturbations such as large scale structure, peculiar velocities, redshift space distortions and future high redshift 21cm surveys. These could all replace our choice of cluster counts as a signal used to break the degeneracy between gravitational potentials. All of these, however, present a number of problems either in their interpretation as biased tracers or in the technological challenges involved in large scale surveys. The observations of clusters on the other hand is a relatively simple procedure and SZ surveys of clusters are a necessary by-product of current and future CMB experiments. The only difficulty involved in this signal is the theoretical modelling required to use them to obtain constraints due to the uncertainty in the choice of mass

functions to be used for theories of modified gravity. In obtaining our forecasted constraints we have only employed the simplest description of phenomenologically modified gravity. The model building for such theories has already shown that there is much more complexity to explore. All models must incorporate a screening mechanism to satisfy standard solar system and laboratory tests of gravity. Screening mechanisms are only one way in which modified gravity models may include significant scale dependence, which we have not taken into account in this work and may provide more testable predictions and therefore more ability to differentiate between models. Concrete models may also lead to modifications to the background expansion, which we have not explored here. This can also lead to additional constraints on model parameters.

The experimental outlook is promising for the observations we have dealt with in this work. Over the next 5-10 years, deviations from GR should be well constrained, and the concordance cosmology will either be more secure or may even have undergone a paradigm shift. A null result would support the concordance cosmology, a conclusion that would be even stronger if dark matter had been detected non-gravitationally by then. A detection of a deviation from GR would be potentially more interesting but would require a completely new theoretical framework and trigger a search for an underlying model for the modifications. Of course, a dark energy model with perturbations may turn out to fit the data just as well and it is not clear at this point whether this degeneracy will ever be broken by observations.

*Acknowledgements* We thank Filipe Abdalla for pointing out the work on self calibration of clusters to us. This work was supported by an STFC studentship.

### Appendix A: Redshift dependent limiting mass for cluster surveys

The full treatment of the limiting mass here is based on [70]. The limiting mass at redshift  $z$ , for a detector at dimensionless frequency  $x$  with a flux limit of  $S_{\text{lim}}$  is given by

$$M_{\text{lim}} = \left( \frac{S_{\text{lim}} d_A^2(z)}{f(x) f_b A_{\text{SZ}} (1+z)} \right)^{\frac{1}{\beta_{\text{SZ}}}}. \quad (\text{A1})$$

Here,  $d_A(z)$  is the angular diameter distance,  $f_b$  is the baryon fraction and  $f(x)$  is the frequency dependence of the SZ effect, given by

$$f(x) = \frac{x^4 e^x}{(e^x - 1)^2} \left( \frac{x(e^x + 1)}{e^x - 1} - 4 \right).$$

The dimensionless frequency is given by  $x = \nu \times \frac{h}{k_B T_{\text{CMB}}}$ , with  $T_{\text{CMB}}$  the temperature of the CMB. For our analysis based on Planck, we used  $S_{\text{lim}} = 30$  mJy and a frequency  $\nu = 353$  GHz. Both  $A_{\text{SZ}}$  and  $\beta_{\text{SZ}}$  are parameters from

Stage I	$z_{\text{mg}} = 30$		$z_{\text{mg}} = 3$		$z_{\text{mg}} = 1$	
Parameter	CMB $\otimes$ WL	CMB $\otimes$ WL + CC	CMB $\otimes$ WL	CMB $\otimes$ WL + CC	CMB $\otimes$ WL	CMB $\otimes$ WL + CC
$\Delta\eta$	$2.6 \times 10^{-2}$	$6.4 \times 10^{-3}(1.5 \times 10^{-2})$	$3.3 \times 10^{-2}$	$1.9 \times 10^{-2}(2.6 \times 10^{-2})$	$1.1 \times 10^{-1}$	$1.1 \times 10^{-1}(1.1 \times 10^{-1})$
$\Delta\mu$	$9.1 \times 10^{-3}$	$3.5 \times 10^{-3}(5.6 \times 10^{-3})$	$1.0 \times 10^{-2}$	$5.0 \times 10^{-3}(7.6 \times 10^{-3})$	$5.1 \times 10^{-2}$	$5.1 \times 10^{-2}(5.1 \times 10^{-2})$

TABLE III: Fisher constraints for time-dependent MGPs for Stage I observations.

the mass-temperature relation for clusters. The values of the constants used here are as follows:  $f_{\text{ICM}} = 0.06$ ,

$$\beta_{\text{SZ}} = 1.75, \text{ and } A_{\text{SZ}} = 3.781 \times 10^8.$$

- 
- [1] G. Dvali, G. Gabadadze, and M. Porrati, *Physics Letters B* **485**, 208 (2000), arXiv:hep-th/0005016.
- [2] P. D. Mannheim, *Astrophys. J.* **561**, 1 (2001), arXiv:astro-ph/9910093.
- [3] M. Milgrom, *Astrophys. J.* **270**, 365 (1983).
- [4] R. H. Sanders, *MNRAS* **363**, 459 (2005), arXiv:astro-ph/0502222.
- [5] T. Jacobson and D. Mattingly, *Phys. Rev. D* **64**, 024028 (2001), arXiv:gr-qc/0007031.
- [6] T. Clifton, P. G. Ferreira, A. Padilla, and C. Skordis, *ArXiv e-prints* (2011), 1106.2476.
- [7] Y. Song and W. J. Percival, *jcap* **10**, 4 (2009), 0807.0810.
- [8] C. Shapiro, S. Dodelson, B. Hoyle, L. Samushia, and B. Flaugher, *Phys. Rev. D* **82**, 043520 (2010), 1004.4810.
- [9] V. Acquaviva and E. Gawiser, *ArXiv e-prints* (2010), 1008.3392.
- [10] E. V. Linder, *Phys. Rev. D* **72**, 043529 (2005), arXiv:astro-ph/0507263.
- [11] L. Wang and P. J. Steinhardt, *Astrophys. J.* **508**, 483 (1998), arXiv:astro-ph/9804015.
- [12] L. Pogosian, A. Silvestri, K. Koyama, and G. Zhao, *Phys. Rev. D* **81**, 104023 (2010), 1002.2382.
- [13] G. Zhao, L. Pogosian, A. Silvestri, and J. Zylberberg, *Physical Review Letters* **103**, 241301 (2009), 0905.1326.
- [14] J. Dossett, M. Ishak, J. Moldenhauer, Y. Gong, and A. Wang, *jcap* **4**, 22 (2010), 1004.3086.
- [15] S. F. Daniel and E. V. Linder, *ArXiv e-prints* (2010), 1008.0397.
- [16] P. Serra, A. Cooray, S. F. Daniel, R. Caldwell, and A. Melchiorri, *Phys. Rev. D* **79**, 101301 (2009), 0901.0917.
- [17] J. Guzik, B. Jain, and M. Takada, *Phys. Rev. D* **81**, 023503 (2010), 0906.2221.
- [18] A. Kosowsky and S. Bhattacharya, *Phys. Rev. D* **80**, 062003 (2009), 0907.4202.
- [19] A. F. Heavens, T. D. Kitchoing, and L. Verde, *MNRAS* **380**, 1029 (2007), arXiv:astro-ph/0703191.
- [20] The Planck Collaboration, *ArXiv Astrophysics e-prints* (2006), arXiv:astro-ph/0604069.
- [21] H. Hoekstra, Y. Mellier, L. van Waerbeke, E. Semboloni, L. Fu, M. J. Hudson, L. C. Parker, I. Tereno, and K. Benabed, *Astrophys. J.* **647**, 116 (2006), arXiv:astro-ph/0511089.
- [22] N. Kaiser, *Society of Photo-Optical Instrumentation Engineers (SPIE) Conference Series* **5489**, 11 (2004).
- [23] The Dark Energy Survey Collaboration, *ArXiv Astrophysics e-prints* (2005), arXiv:astro-ph/0510346.
- [24] J. A. Tyson, *Society of Photo-Optical Instrumentation Engineers (SPIE) Conference Series* **4836**, 10 (2002).
- [25] H. Aihara, C. Allende Prieto, D. An, S. F. Anderson, É. Aubourg, E. Balbinot, T. C. Beers, A. A. Berlind, S. J. Bickerton, D. Bizyaev, et al., *ApJS* **193**, 29 (2011), 1101.1559.
- [26] M. Colless, *Royal Society of London Philosophical Transactions Series A* **357**, 105 (1999), arXiv:astro-ph/9804079.
- [27] E. Bertschinger and P. Zukin, *Phys. Rev. D* **78**, 024015 (2008), 0801.2431.
- [28] M. Kunz and D. Sapone, *Physical Review Letters* **98**, 121301 (2007), arXiv:astro-ph/0612452.
- [29] S. F. Daniel, E. V. Linder, T. L. Smith, R. R. Caldwell, A. Cooray, A. Leauthaud, and L. Lombriser, *Phys. Rev. D* **81**, 123508 (2010), 1002.1962.
- [30] G. Zhao, L. Pogosian, A. Silvestri, and J. Zylberberg, *Phys. Rev. D* **79**, 083513 (2009), 0809.3791.
- [31] A. Lewis, A. Challinor, and A. Lasenby, *Astrophys. J.* **538**, 473 (2000), arXiv:astro-ph/9911177.
- [32] C. Skordis, *Phys. Rev. D* **79**, 123527 (2009), 0806.1238.
- [33] C. Contaldi and D. B. Thomas (in preparation).
- [34] N. Jarosik, C. L. Bennett, J. Dunkley, B. Gold, M. R. Greason, M. Halpern, R. S. Hill, G. Hinshaw, A. Kogut, E. Komatsu, et al., *ApJS* **192**, 14 (2011), 1001.4744.
- [35] M. Manera and D. F. Mota, *MNRAS* **371**, 1373 (2006), arXiv:astro-ph/0504519.
- [36] J. Waizmann and M. Bartelmann, *aap* **493**, 859 (2009), 0804.2815.
- [37] U. Alam, Z. Lukić, and S. Bhattacharya, *ArXiv e-prints* (2010), 1004.0437.
- [38] J. Erlich, B. Glover, and N. Weiner, *jcap* **3**, 6 (2008), 0709.3442.
- [39] R. A. Battye and J. Weller, *Phys. Rev. D* **68**, 083506 (2003), arXiv:astro-ph/0305568.
- [40] S. Basilakos, M. Plionis, and J. A. S. Lima, *ArXiv e-prints* (2010), 1006.3418.
- [41] D. Rapetti, S. W. Allen, A. Mantz, and H. Ebeling, *MNRAS* **406**, 1796 (2010), 0911.1787.
- [42] J. Tang, J. Weller, and A. Zablacki, *ArXiv Astrophysics e-prints* (2006), arXiv:astro-ph/0609028.
- [43] F. Schmidt, *Phys. Rev. D* **80**, 043001 (2009), 0905.0858.
- [44] T. Kobayashi and H. Tashiro, *MNRAS* **398**, 477 (2009), 0903.3738.
- [45] H. Zhao, A. V. Macciò, B. Li, H. Hoekstra, and M. Feix, *apjl* **712**, L179 (2010), 0910.3207.
- [46] B. Li, D. F. Mota, and J. D. Barrow, *ArXiv e-prints* (2010), 1009.1400.
- [47] F. Schmidt, A. Vikhlinin, and W. Hu, *Phys. Rev. D* **80**,

- 083505 (2009), 0908.2457.
- [48] F. Schmidt, Phys. Rev. D **80**, 123003 (2009), 0910.0235.
- [49] A. V. Macciò, C. Quercellini, R. Mainini, L. Amendola, and S. A. Bonometto, Phys. Rev. D **69**, 123516 (2004), arXiv:astro-ph/0309671.
- [50] A. Jenkins, C. S. Frenk, S. D. M. White, J. M. Colberg, S. Cole, A. E. Evrard, H. M. P. Couchman, and N. Yoshida, MNRAS **321**, 372 (2001), arXiv:astro-ph/0005260.
- [51] W. H. Press and P. Schechter, Astrophys. J. **187**, 425 (1974).
- [52] J. R. Bond, S. Cole, G. Efstathiou, and N. Kaiser, Astrophys. J. **379**, 440 (1991).
- [53] R. K. Sheth, H. J. Mo, and G. Tormen, MNRAS **323**, 1 (2001), arXiv:astro-ph/9907024.
- [54] R. K. Sheth and G. Tormen, MNRAS **308**, 119 (1999), arXiv:astro-ph/9901122.
- [55] R. K. Sheth and G. Tormen, MNRAS **329**, 61 (2002), arXiv:astro-ph/0105113.
- [56] R. A. Sunyaev and Y. B. Zeldovich, Comments on Astrophysics and Space Physics **2**, 66 (1970).
- [57] M. L. Norman, ArXiv e-prints (2010), 1005.1100.
- [58] M. Lima and W. Hu, Phys. Rev. D **72**, 043006 (2005), arXiv:astro-ph/0503363.
- [59] R. G. Crittenden and N. Turok, Physical Review Letters **76**, 575 (1996), arXiv:astro-ph/9510072.
- [60] A. Cooray, Phys. Rev. D **65**, 103510 (2002), arXiv:astro-ph/0112408.
- [61] S. Boughn and R. Crittenden, Nature (London) **427**, 45 (2004), arXiv:astro-ph/0305001.
- [62] N. Afshordi, Phys. Rev. D **70**, 083536 (2004), arXiv:astro-ph/0401166.
- [63] P. Corasaniti, T. Giannantonio, and A. Melchiorri, Phys. Rev. D **71**, 123521 (2005), arXiv:astro-ph/0504115.
- [64] T. Giannantonio, R. G. Crittenden, R. C. Nichol, R. Scranton, G. T. Richards, A. D. Myers, R. J. Brunner, A. G. Gray, A. J. Connolly, and D. P. Schneider, Phys. Rev. D **74**, 063520 (2006), arXiv:astro-ph/0607572.
- [65] D. Pietrobon, A. Balbi, and D. Marinucci, Phys. Rev. D **74**, 043524 (2006), arXiv:astro-ph/0606475.
- [66] T. Giannantonio, R. Scranton, R. G. Crittenden, R. C. Nichol, S. P. Boughn, A. D. Myers, and G. T. Richards, Phys. Rev. D **77**, 123520 (2008), 0801.4380.
- [67] A. Cabré, E. Gaztañaga, M. Manera, P. Fosalba, and F. Castander, MNRAS **372**, L23 (2006), arXiv:astro-ph/0603690.
- [68] N. Kaiser, Astrophys. J. **388**, 272 (1992).
- [69] A. Refregier, Ann.Rev.Astron.Astrophys. **41**, 645 (2003), arXiv:astro-ph/0307212.
- [70] J. M. Diego, E. Martínez-González, J. L. Sanz, N. Benítez, and J. Silk, MNRAS **331**, 556 (2002), arXiv:astro-ph/0103512.